Molecular and Cell Biotechnologies

https://doi.org/10.7124/bc.000B2E
UDC 615.015.6:577.27

M.D. Jaaffer, A.M. Chaloop
College of Energy and Environmental Sciences, Al-Karkh University of Science
Baghdad, Iraq
marwa.dawood@kus.edu.iq

DOXORUBICIN-PLGA NANOPARTICLES ARE IMMUNOMODULATORY ANTITUMOR THERAPEUTICS WITH DUAL CYTOTOXIC AND IMMUNE-STIMULATORY EFFECTS

Aim. *The aim of this study is to investigate the immunomodulatory and antitumor effects of doxorubicin-loaded poly(lactic-co-glycolic acid) nanoparticles (DOX-PLGA NPs) designed as a dual-function nano-immunotherapeutic system.* ***Methods.*** *DOX-PLGA NPs were synthesized by the emulsion-solvent evaporation method and characterized for particle size, zeta potential, morphology (TEM), drug loading, and release behavior. The cytotoxicity of free DOX and DOX-PLGA NPs was evaluated in MCF-7 and HCT116 cancer cell lines using the MTT assay. «Peripheral blood mononuclear cell (PBMC) – tumor» co-cultures were analyzed for cytokine secretion (IFN-γ, IL-2, TNF-a, and IL-10) and immune cell subsets ($CD8^+$ T-cells, NK cells, and macrophage polarization). The therapeutic efficacy was further examined in CT26 tumor-bearing mice.* ***Results.*** *The DOX-PLGA NPs exhibited a mean size of approximately 145 nm (PDI 0.18, ζ −22 mV), with a drug loading efficiency of 12.5% and encapsulation efficiency of 78%. In comparison to free DOX, the nano-formulation lowered cell viability to a greater extent ($p < 0.01$) and stimulated greater release of IFN-γ, IL-2, and TNF-a, while IL-10 levels decreased. Flow cytometric analysis shows increases in the populations of $CD8^+$ T and NK cells and a congruent macrophage reversal to the M1 macrophage phenotype. Tumor growth was markedly suppressed, survival was extended, and DOX-PLGA NPs produced insignificant systemic toxicity in the in vivo setting.* ***Conclusions.*** *The immuno-nanoparticles demonstrate controlled release of DOX-PLGA NPs while maintaining powerful immune stimulation due to the dual cytotoxic and immunostimulatory effects they exhibit. Their application as a novel platform for nano-immunotherapy in the treatment of cancer is justified.*

Keywords: *DOX-loaded PLGA nanoparticles; PLGA; nano-immunotherapy; cytokines; immune activation; cancer therapy.*

Citation: Jaaffer M.D., Chaloop A.M. (2026) Doxorubicin-PLGA nanoparticles are immunomodulatory antitumor therapeutics with dual cytotoxic and immune-stimulatory effects. *Biopolymers & Cell*, 1(42), 54—67. https://doi.org/10.7124/bc.000B2E

Introduction

Cancer is still one of the major health problems around the world, with millions of deaths every year, even with major improvements in diagnosis and treatment [1]. Standard treatments like chemotherapy and radiotherapy are limited by tumor heterogeneity, the development of drug resistance, and significant systemic toxicity [2]. Immunotherapy has captured the attention of the medical community. In recent years, increasing attention has been directed toward harnessing the immune system to develop new and more effective approaches for cancer treatment [3]. Still, poorly controlled tumor immune evasion and the elaborate immunosuppressive tumor microenvironment (TME) create significant challenges to the efficacy of immunotherapy [4].

Nanotechnology offers a way to surpass these shortcomings. Nanoparticle-based drug delivery systems (NP-DDS) can improve the pharmacokinetic profile of drugs, extend their circulation time, increase their accumulation in tumor tissues, and reduce systemic toxicity [5]. NP-DDS can also act beyond passive carriers, as far as immune response is concerned, by augmenting antigen presentation, activating CTLs and NK cells, and switching macrophages to a pro-inflammatory state [6, 7].

The integration of nanotechnology with immunotherapy has given rise to innovations with the development of nano-immunotherapy, an integrated approach that utilizes nanomaterials to enhance antitumor immunity and address the limitations of traditional immunotherapy [8—10]. While advances have been made, there is a need to fully comprehend the interplay of nanoparticles, the immune system, and the tumor microenvironment to refine the design of nanoparticles for the greatest therapeutic impact [11, 12]. The current study aims to expand existing knowledge about the immunomodulatory and anti-tumor potential of DOX-PLGA NPs, with particular emphasis on how they stimulate anti-tumor immune responses and exert therapeutic effects in both *in vitro* and *in vivo* models.

Materials and Methods

Chemicals and Reagents

Doxorubicin hydrochloride (DOX), polyvinyl alcohol (PVA; 87—89% hydrolyzed), dichloromethane (DCM; ≥99.9%), dimethyl sulfoxide (DMSO; ≥99.9%), and phosphate-buffered saline (PBS; pH 7.4) were all purchased from Sigma-Aldrich (St. Louis, MO, USA). Poly(lactic-co-glycolic acid) (PLGA; 50:50, MW ≈ 30,000—60,000 Da) was obtained from the same supplier. All solutions and preparations were carried out using ultrapure water (resistivity = 18.2 MΩ × cm) obtained from a Milli-Q purification system.

Nanoparticle Preparation

DOX-loaded PLGA nanoparticles (DOX-PLGA NPs) were prepared using a modified emulsion-solvent evaporation method [13]. PLGA (poly lactic-co-glycolic acid); 50:50, MW 30,000—60,000 Da; Sigma-Aldrich) was used as the biodegradable polymeric matrix for nanoparticle formulation. PLGA (10 mg/mL) and doxorubicin hydrochloride were co-dissolved in dichloromethane (organic phase) at a polymer-to-drug mass ratio of 10:1, unless otherwise specified. The organic phase was added dropwise into a 2% (w/v) polyvinyl alcohol (PVA) aqueous solution (volume ratio 1:10) under probe sonication (40% amplitude, 2 × 60 s) in an ice bath to obtain a stable emulsion. The emulsion was magnetically stirred overnight at room temperature to allow complete solvent evaporation. The nanoparticles were then collected by centrifugation at 15,000 rpm for 20 min at 4 °C, washed three times with deionized water, and lyophilized (−55 °C, 0.05 mbar) in the presence of 5% mannitol as a cryoprotectant. Macroscopically, the formulations displayed distinct appearances (Fig. 1): the free DOX solution appeared bright red and transparent, blank PLGA nanoparticles formed a nearly colorless milky suspension, whereas the DOX-PLGA NPs produced a turbid reddish suspension, confirming efficient drug encapsulation within the polymer matrix.

Physicochemical Characterization

Morphology: Transmission electron microscopy (TEM; JEOL JEM-2100, Japan) operating at 200 kV was used to analyze the nanoparticles' morphology and surface features. To visualize particle shape and dispersion uniformity, a drop of the nanoparticle suspension was placed on a carbon-coated copper grid, negatively stained with 2% (w/v) uranyl acetate, air-dried, and then imaged.

Drug Loading and Encapsulation Efficiency: DOX quantification involved UV-visible spectrophotometry (Shimadzu UV-1800, Japan) at the absorption spectrum peak of 480 nm. Using a standard series of DOX solutions (R^2 = 0.999), constructed calibration curves, and correcting the absorbance values for blank PLGA nanoparticles allowed for proper calculations. Subsequently, using standard equations for the total and incorporated DOX content, the drug loading (DL %) and encapsulation efficiency (EE% %) for the formulated PLGA nanoparticles were evaluated.

Fourier-Transform Infrared (FTIR) and X-Ray Diffraction (XRD) Analyses: FTIR spectra were recorded using a Bruker Tensor-27 spectrometer within the range of 4000—500 cm^{-1} to characterize the potential interactions between the functional groups of DOX and PLGA. For the purpose of evaluating the crystalline or amorphous nature of DOX before and after encapsulation, X-ray diffraction patterns were made using a PANalytical X'Pert PRO diffractometer with Cu-Kα radiation (λ = 1.5406 Å) at 2θ = 5—60°.

***In Vitro* Drug Release Study:** The release behavior of DOX from nanoparticles was evaluated using a dialysis method. A defined quantity of DOX-PLGA NPs (equivalent to 2 mg DOX) was placed in a dialysis bag (MWCO = 10 kDa) and immersed in 50 mL of PBS (pH 7.4) containing 0.1% Tween-80 at 37 °C under gentle stirring (100 rpm). At predetermined time intervals up to 72 h, aliquots were withdrawn and replaced with equal volumes of fresh buffer. The concentration of released DOX was determined spectrophotometrically at 480 nm, and the cumulative percentage release was calculated relative to the total drug content obtained after nanoparticle lysis in DMSO.

Cell Lines and Culture Conditions

Human breast adenocarcinoma (MCF-7) and colorectal carcinoma (HCT116) cell lines were obtained from the American Type Culture Collection (ATCC, USA). The cells were maintained in Dulbecco's Modified Eagle Medium (DMEM; Gibco, USA) supplemented with 10% (v/v) heat-inactivated fetal bovine serum (FBS; Sigma-Aldrich), 100 U/mL penicillin, and 100 μg/mL streptomycin. The cultures were incubated at 37 °C in a humidified atmosphere containing 5% CO_2. The cells were used between passages 5 and 20, verified by short tandem repeat (STR) profiling, and routinely confirmed to be mycoplasma-free using a PCR-based detection kit (tested monthly).

In Vitro Cytotoxicity (MTT Assay)

Cell viability was assessed using the MTT colorimetric assay. Briefly, MCF-7 and HCT116 cells were seeded in 96-well plates at a density of 1×10^4 cells per well in 100 μL of complete medium and allowed to adhere for 24 h. The cells were then treated with vehicle control, free DOX, blank PLGA nanoparticles, or DOX-loaded PLGA nanoparticles (DOX-PLGA NPs) at concentrations equivalent to 0.1—100 μg/mL of DOX. DOX and DOX-PLGA nanoparticles were used at different concentrations of 0.1 to 100 μg/mL. Nonlinear regression of dose response curves was used to determine IC_{50} values, which were used in determine doses of treatment where appropriate. After 48 h of exposure, 20 μL of MTT solution (5 mg/mL in PBS) was added to each well and incubated for 4 h at 37 °C. The medium was carefully removed, and the resulting formazan crystals were dissolved in 150 μL of DMSO. Absorbance was measured at 570 nm with a reference wavelength of 630 nm using a Bio-Rad microplate reader. Cell viability (%) was calculated according to the equation:

$$A\left\{\text{treated}\right\} / A\left\{\text{control}\right\} \times 100$$

The half-maximal inhibitory concentration (IC_{50}) values were determined by nonlinear four-parameter logistic regression using GraphPad Prism 8 software. All experiments were performed independently three times, with each treatment condition tested in six replicate wells (n = 6).

Immunological Assays

Isolation and Co-culture of PBMCs: Peripheral blood mononuclear cells (PBMCs) were obtained from healthy adult volunteers by density gradient centrifugation using Ficoll-Paque PLUS (GE Healthcare, Sweden). Tumor cells (MCF-7 and HCT116) were pretreated for 24 h with free DOX, blank PLGA nanoparticles, or DOX-loaded PLGA nanoparticles (DOX-PLGA NPs). After treatment, the cells were thoroughly washed with PBS and co-cultured with freshly isolated PBMCs in complete RPMI-1640 medium supplemented with 10% FBS at an effector-to-target (E: T) ratio of 10:1. This was done with MCF-7 and HCT116 cells (24 h) at concentrations of 0.1—100 μg/ml DOX control, blank PLGA nanoparticles, or DOX-PLGA nanoparticles and then washed and resuspended to co-culture. Tumor cells were co-incubated with PBMCs at 37 °C in a humidified incubator with 5% CO2 at a density of 1×10^6 cells/well in a 24-well plate.

Cytokine Quantification (ELISA): The concentrations of IFN-γ, IL-2, TNF-α, and IL-10 in culture supernatants were quantified using commercially available ELISA kits (R&D Systems, USA) according to the manufacturer's instructions. Standard curves were generated in duplicate for each cytokine on every assay plate. The results were expressed as mean ± SEM of triplicate independent experiments.

Flow Cytometric Analysis of Immune Subsets: Immune cell phenotyping was performed using fluorochrome-conjugated monoclonal antibodies specific for CD3, CD4, CD8, CD56, and CD11b (BD Biosciences, USA; detailed in Table 1). Data acquisition was carried out on a BD FACSCalibur flow cytometer equipped with appropriate compensation and fluorescence-minus-one (FMO) controls. A minimum of 30,000 events were recorded for each sample. Data analysis was performed in FlowJo v10 (Tree Star, USA) using a predefined gating strategy by an independent, blinded analyst.

Amount per test: The amount of antibody applied to1×10^6 cells in 100 μL of staining buffer (unless indicated otherwise by the manufacturer). **Staining conditions:** Staining was done in the

Table 1. **Flow cytometric immune phenotyping monoclonal antibodies**

Marker	Immune cell subset	Clone	Fluorochrome	Manufacturer	Catalog No.	Host / Isotype	Amount per test*
CD3	Total T lymphocytes	UCHT1	FITC	BD Biosciences (USA)	555332	Mouse IgG1 κ	5 μL
CD4	Helper T cells	RPA-T4	PE	BD Biosciences (USA)	555347	Mouse IgG1 κ	5 μL
CD8	Cytotoxic T cells	RPA-T8	PerCP-Cy5.5	BD Biosciences (USA)	560662	Mouse IgG1 κ	5 μL
CD56	Natural killer (NK) cells	NCAM16.2	APC	BD Biosciences (USA)	555518	Mouse IgG1 κ	5 μL
CD11b	Myeloid cells / Monocytes	ICRF44	PE	BD Biosciences (USA)	557743	Mouse IgG1 κ	5 μL

dark for 20 min at 4 °C. Gating was done using fluorescence-minus-one (FMO) controls.

In Vivo Tumor Model

Female BALB/c mice (6—8 weeks old, 20—25 g) were obtained from the institutional animal facility and maintained under specific pathogen-free (SPF) conditions (temperature 22 ± 2 °C, relative humidity 55 ± 10%, 12 h light/dark cycle) with free access to standard food and water. All experimental procedures were conducted in accordance with institutional ethical guidelines for the care and use of laboratory animals.

To establish the tumor model, each mouse was subcutaneously injected in the right flank with 1×10^6 CT26 murine colon carcinoma cells suspended in 100 μL of sterile PBS. When tumors reached approximately 100 mm^3, animals were randomly assigned using computer-generated block randomization into four groups (6 per group, total 24) assigned the following: 1) saline control, 2) free DOX, 3) blank PLGA nanoparticles, and 4) DOX-loaded PLGA nanoparticles (DOX-PLGA NPs). Each treatment was given by IV with a DOX-equivalent of 5 mg/kg every three days for a total of three weeks. Tumor size was assessed with digital calipers three times a week, and the volume (V) was derived from the equation: volume $V = (\text{length} \times \text{width}^2) / 2$.

Monitoring for systemic toxicity was done by observing body weight and appearance. All tumor size and histopathology assessments were done by blinded, independent evaluators who were unaware of the treatment groups. Animals with humane endpoints (tumor ulceration, ≥15% body weight loss, or tumor volume ≥1500 mm^3) were humanely euthanized.

Histopathology and Immunohistochemistry

The excised tumors were fixed in 10% neutral buffered formalin for 24 hours, then dehydrated in gradated ethanol, and embedded in paraffin wax as follows. With a rotary microtome, 5 μm-thick sections were made and placed on glass slides. For the general histological evaluation, the tumors with associated necrotic regions were assessed with the standard Hematoxylin and Eosin (H&E) staining to obtain the morphology.

For the immunohistochemical (IHC) assays, the sections underwent a series of deparaffinization, rehydration, and antigen retrieval in a citrate buffer (pH 6.0) for 20 min at 95 °C. Quenching of the endogenous peroxidase activity was done with 3% hydrogen peroxide for 10 min. The sections were blocked and then incubated overnight at 4 °C with primary antibodies against CD8 (1:200 dilution) and NKp46 (1:150 dilution) for cytotoxic T lymphocytes and natural killer cells, respectively. After washing, the slides were incubated with horseradish peroxidase (HRP)-conjugated secondary antibodies, and then the cells were visualized with 3,3'-diaminobenzidine (DAB) chromogen. Hematoxylin was used to counterstain the nuclei. The quantification of the positive immune cells was done in a random selection of five high-power fields (HPF, 400×) per section using the ImageJ software (v1.54, NIH, USA), and the results were expressed as the mean of positive cells per HPF.

Statistical Analysis

All values are expressed as mean ± standard deviation (SD), unless otherwise stated. Normality was examined using the Shapiro-Wilk test. Comparisons of mean differences among multiple groups were performed using one-way analysis of variance (ANOVA), accompanied by Tukey's post hoc test for endpoint analyses. Longitudinal tumor growth data were assessed using two-way repeated measures ANOVA with the Greenhouse-Geisser correction. Non-parametric data were assessed using the Kruskal-Wallis test with Dunn's multiple comparisons correction. Exact values of p are reported for all analyses, with significance set at $p < 0.05$. All statistical analyses were performed, and all graphs were made using GraphPad Prism, version 8.0 (GraphPad Software, USA). Technical replicates are described within each assay, whereas

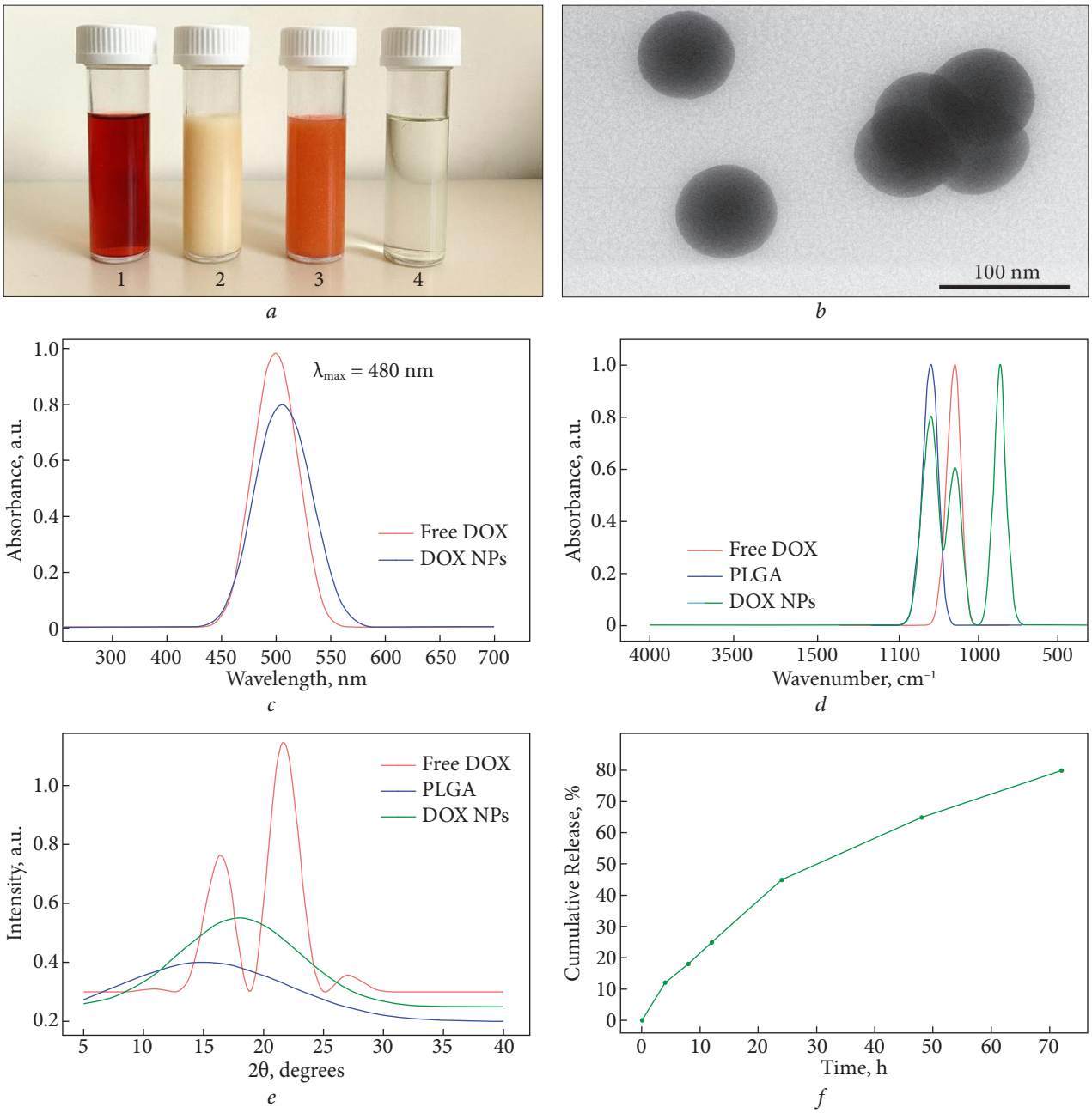

Fig. 1. Physicochemical characterization of DOX-PLGA NPs. *a* — Various formulations' appearances: free DOX (red), blank PLGA nanoparticles (milky white), DOX-PLGA nanoparticles (turbid reddish), and control solvent (clear). *b* — Transmission electron micrograph (TEM) of spherical DOX-PLGA NPs with smooth surfaces (scale bar = 100 nm). *c* — UV-Vis absorption spectra of free DOX **(red)** and DOX-PLGA NPs **(blue),** showing encapsulation-induced red-shift of DOX peak (~480 nm). *d* — FTIR spectra of free DOX, PLGA, and DOX-PLGA NPs. Discrimination of key PLGA (1755 cm^{-1}, 1095 cm^{-1}) and DOX (1610 cm^{-1}, 1285 cm^{-1}) bands indicates drug-polymer interaction. *e* — X-ray diffraction (XRD) patterns of free DOX, PLGA, and DOX-PLGA NPs; disappearance of DOX crystalline peaks suggests polymer matrix drug dispersion (amorphous). *f* — *In vitro* cumulative DOX release profile from DOX-PLGA NPs in PBS (pH 7.4, 37 °C) showing biphasic release (sustained release of ~25% during 12h burst) to 72h. Data presented as mean ± SD (n = 3); $R^2 > 0.999$

biological replicates-referring to independent experiments or individual animals are described as the sample size (n).

Ethics Statement

All experiments involving animals were conducted according to the national regulations related care and use of laboratory animals in Iraq, as well as the International Guidelines for the ethical use of animals in research. When this study was conducted, Al-Karkh University of Science did not yet have an Institutional Animal Ethics Committee. However, as noted in the text, this did not mean that the research had no regard for the animals. Procedures were designed to safeguard the well-being of the animals and, for ethical reasons, an adequate, though not excessive, number of animals was used to derive statistically valid conclusions. Research involving human peripheral blood mononuclear cells (PBMCs) was conducted in accordance to the ethical guidelines of the Declaration of Helsinki (2013 revision). Written informed consent was obtained from all healthy adult donors before blood collection, and, in accordance with ethical standards, identifiers were removed to protect the confidentiality of the subjects.

Results and Discussion

Nanoparticle Preparation and Characterization

The DOX-PLGA NPs were created using the emulsion-solvent evaporation method, exhibiting positive attributes all around, avoiding negative functional. When treated, the formulations were successful: while free DOX was observed as a red solution, blank PLGA NPs were a milky suspension. The DOX-PLGA NPs were a turbid reddish suspension (Fig. 1*a*). The surfaces of the suspended NPs were smooth and spherical with 100—200 nm as revealed with TEM analysis (Fig. 1*b*). This is ideal for tumor accumulation due to the EPR effect (enhanced permeability and retention effect). UV-Vis was performed determined that free DOX had an absorption peak around 480 nm, while blank NPs were around 0. The red shift and broadened peak as observed in the DOX-PLGA NPs (Fig. 1*c*) determined that DOX was retained in the polymeric matrix as the peak. The loading capacity and encapsulation efficiency were 12.5 ± 1.3% and 78 ± 4% (respectively; n = 3, $R^2 > 0.999$). FTIR spectra displayed attenuated DOX-specific peaks (1610 and 1285 cm^{-1}) together with distinct PLGA bands (1755 and 1095 cm^{-1}), verifying non-covalent drug-polymer interactions (Fig. 1*d*). XRD patterns of free DOX exhibited sharp crystalline reflections, whereas DOX-PLGA NPs showed an amorphous halo similar to blank PLGA NPs (Fig. 1*e*), indicating molecular-level dispersion and improved physical stability [4]. The *in vitro* release profile exhibited an initial burst release of ≈25% within 12 h, followed by sustained release reaching ≈80% after 72 h (Fig. 1*f*). Such controlled release ensures prolonged therapeutic action with reduced systemic toxicity [16]. Collectively, these results confirm that DOX-PLGA NPs possess optimal particle size,

Table 2. **IC_{50} and cell viability (%) of MCF-7 and HCT116 cells, 48 h after treatment with free DOX and DOX-PLGA NPs**

Treatment group	IC 50, MCF-7, (μg/ml)	IC 50, HCT116, (μg/ml)	Cell viability at 10, μg/ml (%)
Free DOX	7.4 ± 0.5	6.7± 0.3	45 ± 4
DOX-NPs	3.1 ± 0.2	2.8 ± 0.1	28 ± 2
Blank NPs	–	–	~100
Control	–	–	100

Note: Values represent mean ± standard deviation (n = 3). IC_{50} values were calculated from nonlinear regression of dose-response curves using GraphPad Prism v9. Statistical analysis: one-way ANOVA followed by Tukey's post-hoc test (*$p < 0.05$ considered significant).

morphology, and encapsulation efficiency for controlled anticancer drug delivery [14—17].

In Vitro Cytotoxicity

The cytotoxic ability of DOX-PLGA NPs was evaluated in human breast (MCF-7) and colorectal (HCT116) cancer cells using the MTT assay (Fig. 2). Both free DOX and DOX-PLGA NPs exhibited a dose-dependent reduction in viability across tested concentrations (0.1—100 μg/mL). DOX-PLGA NPs showed greater cytotoxicity than free DOX, likely due to increased cell uptake and sustained drug release. After 48 hours, cell viability in the DOX-PLGA NPs group was 28 ± 3%, compared to 45 ± 5% in the free DOX group ($p < 0.01$). Blank PLGA NPs caused less than 5% reduction in viability, confirming their biocompatibility (Table 2). This demonstrates the enhanced antiproliferative activity of DOX, along with reduced cytotoxic effects due to PLGA encapsulation.

Interestingly, the calculated IC_{50} values further confirmed the enhanced potency of DOX-PLGA NPs compared with free DOX in both cell lines. The IC_{50} of DOX-PLGA NPs was 3.1 ± 0.2 μg/mL in MCF-7 and 2.8 ± 0.1 μg/mL in HCT116, whereas free DOX exhibited significantly higher IC_{50} values of 7.4 ± 0.5 μg/mL and 6.7 ± 0.3 μg/mL, respectively. This improvement in cytotoxic efficiency is due to enhanced intracellular absorption and extended drug release from the nanoparticle matrix, both of which help to overcome efflux-mediated drug resistance that was previously observed for conventional DOX formulations [17, 18].

Cytokine production

ELISA analysis showed that DOX-PLGA NPs significantly increased the secretion of pro-inflammatory cytokines when compared to free DOX (Fig. 3, Table 3). In particular, DOX-PLGA NPs reduced the level of the immunosuppressive cytokine IL-10 by over 35% while increasing IFN-γ production by around 3.2—8 times, IL-2 by 2.5—5 times, and TNF-α by roughly two times. These results indicate

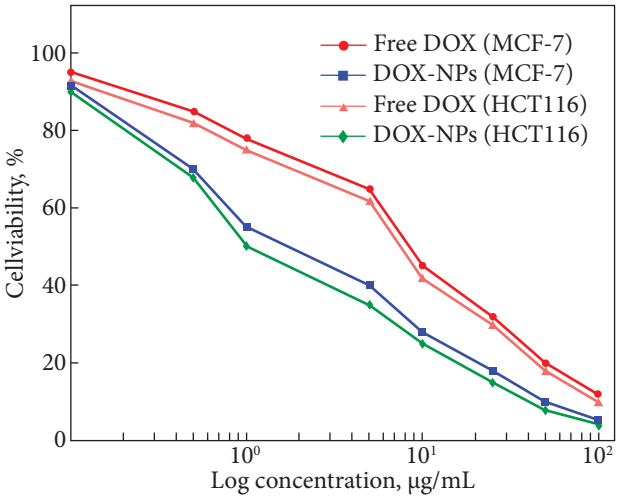

Fig. 2. DOX cytotoxicity and DOX-PLGA NPs after 48 h incubation on MCF-7 and HCT116 at each of the concentrations (0.1—100 μg/mL). The same was also done using blank PLGA nanoparticles. The data are reported as mean SD (n = 3). One-way ANOVA and post-hoc test ($p < 0.05$) in the form of statistical analysis were used

that DOX-PLGA NPs not only preserve the cytotoxicity of DOX but also potentiate Th1-type immune activation within the tumor-immune microenvironment ($p < 0.01$ versus free DOX).

Taken together, these findings indicate that the mechanism of action of DOX-PLGA NPs is dual in nature: **(i)** a direct cytotoxic effect on tumor cells, leading to growth inhibition and apoptosis, and **(ii)** an indirect immunomodulatory effect through reprogramming the tumor-immune

Table 3. **The concentration of cytokines (pg/mL) in PBMC-tumor co-cultures following 48 h treatment with free DOX and DOX-PLGA NPs (mean ± SEM, n = 3)**

Cytokine	Control	Free DOX	DOX-PLGA NPs
IFN-γ	50 ± 5	120 ± 10	380 ± 20
IL-2	25 ± 3	60 ± 6	150 ± 12
TNF-α	30 ± 4	75 ± 7	160 ± 15
IL-10	40 ± 4	35 ± 3	26 ± 3

Note: Data are mean ± SEM (n = 3). Cytokine levels determined by ELISA in PBMC-tumor co-culture supernatants. $p < 0.01$ was considered significant versus free DOX.

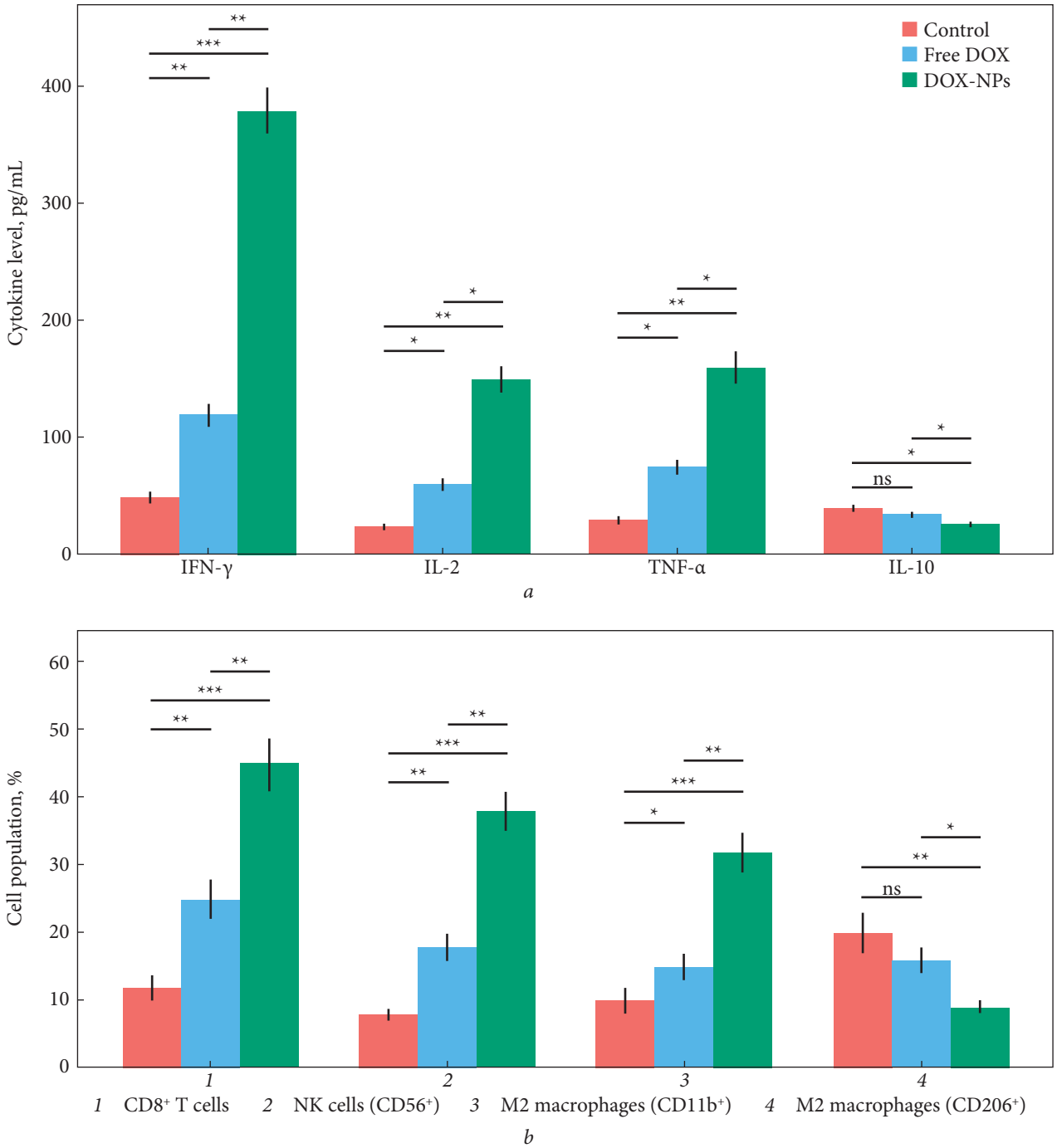

Fig. 3. *a* — Cytokine release profile (IFN-γ, IL-2, TNF-α, and IL-10) in PBMC-tumor co-cultures after 48 h of treatment. *b* — Flow cytometric analysis of immune cell with control, free DOX, and DOX-PLGA NPs (mean ± SEM, n = 3 cytometric analysis of immune cell subsets 48 h post-treatment, displaying exemplary gating and quantification of the populations of M1 and M2 macrophages, CD8 T cells, and NK cells in the various treatment groups. Data are presented as mean ± SEM (n = 3). Statistical analysis was performed using one-way ANOVA followed by Tukey's post-hoc test (* — $p < 0.05$, ** — $p < 0.01$, *** — $p < 0.001$ vs. control)

microenvironment toward a pro-inflammatory, antitumor phenotype. This immune reprogramming is characterized by enhanced secretion of Th1-type cytokines (IFN-γ, IL-2, TNF-α) and reduced levels of the immunosuppressive cytokine IL-10, which collectively promote activation of cytotoxic $CD8^+$ T cells, NK cells, and M1 macrophages. Similar immune-potentiating effects of nanoparticle based drug delivery systems have been documented in recent nano-immunotherapy studies [19, 20]. As for the immune activation evident in the results of this study, it is probably the result of direct and indirect mechanisms. DOX-PLGA NPs directly engage immune cells and trigger the activation of pattern recognition receptors and M1 polarization. Indirectly, however, through nanoparticle-mediated tumor cell apoptosis, DAMPs such as HMGB1 and ATP can fuel the recruitment of $CD8^+$ T cells and NK cells in the tumor microenvironment. The coordinated action of these pathways explains the simultaneous chemotherapeutic and immunomodulatory effect [21, 22].

Immune Cell Activation (Flow Cytometry). Flow cytometry analysis

Flow cytometric profiling revealed that immune cell responses were significantly enhanced following treatment with DOX-PLGA NPs compared with the free DOX and control groups. In particular, the percentage of $CD56^+$ natural killer (NK) cells increased by over 38%, while the proportion of $CD8^+$ cytotoxic T lymphocytes increased by around 45% compared to the control ($p < 0.01$). Additionally, macrophage polarization analysis showed a decrease in the immunosuppressive M2 subgroup ($CD206^+$) and a strong shift toward the pro-inflammatory M1 phenotype ($CD11b^+$). Table 4 summarizes these quantitative results, and Fig. 3*b* provides a pictorial representation.

Antitumor immunity depends largely on the effectiveness of $CD8^+$ cytotoxic T lymphocytes and NK cells. Classically activated M1 macrophages also support tumor eradication through the secretion of pro-inflammatory cytokines and the stimulation of the adaptive immune system [23, 24]. All of this evidence leads to the conclusion that the DOX-PLGA NPs are dual-functional, exhibiting strong chemotherapy and immunomodulatory properties [25]. The interplay of these two functions leads to considering them advanced therapeutic nano-immunotherapy tools with the ability to provide tumor cytotoxic effects and reprogram the immune system.

The enhancement of pro-inflammatory cytokines in the presence of doxorubicin, which has intrinsic cytostatic properties, relates to the nanoparticle-mediated delivery system that alters the pharmacodynamics of the drug. PLGA encapsulation of DOX softens the acute cytotoxicity of the drug on immune cells by reducing the intracellular concentration, allowing sufficient immune cell viability for cytokine secretion. In addition, the sustained release of the drug and phagocytosis of nanoparticles by antigen-presenting cells are likely to be positive contributors to ICD of tumor cells and secondary activation of effector lymphocytes. [21, 22].

In Vivo Antitumor Efficacy

The therapeutic efficacy of DOX-PLGA NPs was evaluated in a CT26 murine colon carcinoma model. Tumor growth analysis demonstrated that DOX-PLGA NPs exerted a markedly stronger

Table 4. **Flow cytometry of immune cytokine activation of PBMC-tumor co-cultures 48 h post-treatment. The data are presented as mean ± SEM (n = 3)**

Cell type/marker	Control	Free DOX	DOX-PLGA NPs
$CD8^+$ T cells (%)	12 ± 2	25 ± 3	45 ± 4
NK cells ($CD56^+$, %)	8 ± 1	18 ± 2	38 ± 3
M1 macrophages ($CD11b^+$, %)	10 ± 2	15 ± 2	32 ± 3
M2 macrophages ($CD206^+$, %)	20 ± 3	16 ± 2	9 ± 1

Note: Values represent mean ± SEM (n = 3). Statistical analysis was performed using one-way ANOVA followed by Tukey's post-hoc test.

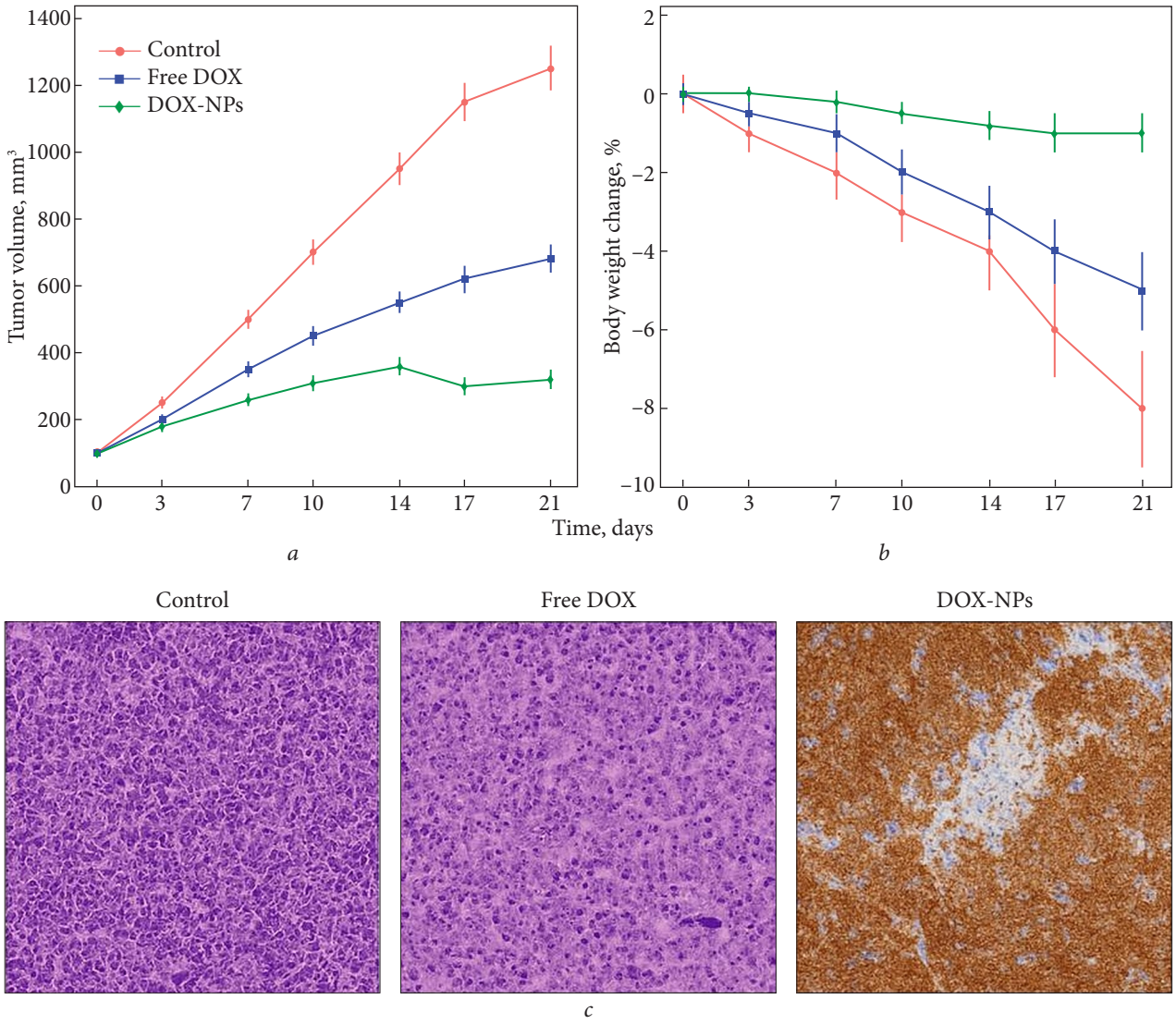

Fig. 4. Representative histological sections of tumor tissues. *a* — Control showing dense tumor cells with minimal immune infiltration. *b* — Free DOX showing scattered $CD8^+$ T lymphocytes (black arrows). *c* — DOX-PLGA NPs showing marked NK cell infiltration (red arrows), highlighted by brown immunostaining. Scale bar: 50 μm

inhibitory effect on tumor progression compared with both free DOX and saline-treated controls ($p < 0.01$). After 21 days of treatment, the mean tumor volume in the DOX-PLGA NP group was also 320 ± 25 mm^3, considerably less than the free DOX group (680 ± 40 mm^3) and the saline control (1250 ± 65 mm^3) (Fig. 4*a*).

There were also no significant changes in body weight or overt signs of systemic toxicity in mice treated with DOX-PLGA NPs. The Physician ensured and recorded biocompatibility and tolerability (Fig. 4*b*). The control and free DOX groups had malignant tumors with histopathologic and H&E stains showing necrotic cells, and tumor-free DOX and control groups had viable malignant regions. Moreover, immunohistochemical analysis showed pronounced infiltration of $CD8^+$ T lymphocytes and NK cells within the tumor microenvironment

of DOX-PLGA NP-treated mice (Fig. 4*c*). These *in vivo* observations are consistent with the *in vitro* immunological findings and further confirm the dual chemotherapeutic and immunomodulatory nature of the DOX-PLGA NPs [26, 27].

Conclusions

DOX-conjugated PLGA nanoparticles demonstrated dual antitumor functionality by integrating controlled chemotherapeutic delivery with potent immunomodulatory activity. Compared with free DOX, the nanoformulation significantly enhanced the secretion of pro-inflammatory cytokines, increased $CD8^+$ T lymphocytes and NK cell populations, and repolarized macrophages toward the M1 phenotype. A significant decrease in tumor growth and increased immune cell penetration into the tumor microenvironment *in vivo* was observed along with these immunological effects. All of these results emphasize the potential of this nano-immunotherapeutic approach for direct cell-killing and immune system activation simultaneously. Further research should incorporate complete profiling of pharmacokinetics, biodistribution, and prolonged biosafety, along with optimal formulation parameters focused on synergistic testing with immune checkpoint inhibitors, to allow these findings to advance into the clinic faster.

Funding. No specific funding was acquired for this research from any public, commercial, or not-for-profit funding agency. All the experimental and analytical work was conducted using institutional facilities and the authors' own resources.

Conflict of Interest. The authors declares no conflict of interest.

Author Contributions. Conceptualization: Marwa D. Jaaffer, Methodology: Ammar M. Chaloop. Investigation: Ammar M. Chaloop. Data Curation: Ammar M. Chaloop. Writing — Original Draft: Ammar M. Chaloop, Marwa D. Jaaffer. Writing — Review and Editing: Marwa D. Jaaffer, Ammar M. Chaloop. The final manuscript was approved and read by all authors.

REFERENCES

1. *Sung H, Ferlay J, Siegel RL, et al., and Bray F.* Global Cancer Statistics 2020: GLOBOCAN Estimates of Incidence and Mortality Worldwide for 36 Cancers in 185 Countries. *CA Cancer J Clin.* 2021; **71**(3):209—49.
2. *Senapati S, Mahanta AK, Kumar S, Maiti P.* Controlled drug delivery vehicles for cancer treatment and their performance. *Signal Transduct Target Ther.* 2018; **3**(7):1—19.
3. *Mellman I, Coukos G, Dranoff G.* Cancer immunotherapy comes of age. *Nature.* 2011; **480**(7378):480—9.
4. *Binnewies M, Roberts EW, Kersten K, et al., and Krummel MF.* Understanding the tumor immune microenvironment (TIME) for effective therapy. *Nat Med.* 2018; **24**(5):541—50.
5. *Blanco E, Shen H, Ferrari M.* Principles of nanoparticle design for overcoming biological barriers to drug delivery. *Nat Biotechnol.* 2015; **33**(9):941—51.
6. *Irvine DJ, Swartz MA, Szeto GL.* Engineering synthetic vaccines using cues from natural immunity. *Nat Mater.* 2013; **12**(11):978—90.
7. *Wang Y, Xu Z, Chen Y, et al., and Gu Z.* Nanoparticle-based delivery system for cancer immunotherapy. *Nano Lett.* 2020; **20**(9):5579—92.
8. *Riley RS, June CH, Langer R, Mitchell MJ.* Delivery technologies for cancer immunotherapy. *Nat Rev Drug Discov.* 2019; **18**(3):175—96.
9. *Danhier F, Ansorena E, Silva JM, et al., and Préat V.* PLGA-based nanoparticles: an overview of biomedical applications. *J Control Release.* 2012; **161**(2):505—22.
10. *Kumari A, Yadav SK, Yadav SC.* Biodegradable polymeric nanoparticles based drug delivery systems. *Colloids Surf B Biointerfaces.* 2010; **75**(1):1—18.
11. *Sahoo SK, Labhasetwar V.* Nanotech approaches to drug delivery and imaging. *Drug Discov Today.* 2003; **8**(24):1112—20.
12. *Alexis F, Pridgen EM, Langer R, Farokhzad OC.* Nanoparticle technologies for cancer therapy. *Handb Exp Pharmacol.* 2010; **197**:55—86.

13. *Mosmann T.* Rapid colorimetric assay for cellular growth and survival: application to proliferation and cytotoxicity assays. *J Immunol Methods.* 1983; **65**(1—2):55—63.
14. *Freshney RI.* Culture of animal cells: a manual of basic technique and specialized applications.– Hoboken: "Wiley-Blackwell", 2015;728p.
15. *Peer D, Karp JM, Hong S, et al., and Langer R.* Nanocarriers as an emerging platform for cancer therapy. *Nat Nanotechnol.* 2007; **2**(12):751—60.
16. *Kim J, Choi Y, Yang S, et al., and Kim K.* Sustained and long-term release of doxorubicin from PLGA nanoparticles for eliciting anti-tumor immune responses. *Pharmaceutics.* 2022; **14**(3):474.
17. *Wu J, Wang X, Wang Y, et al., and Li S.* Application of PLGA in Tumor Immunotherapy. *Polymers (Basel).* 2024; **16**(9):1253.
18. *Al-Thani AN, et al.* Next-generation nanoparticles for cancer and autoimmune disorders. *Biochem J.* 2025; **482**(2):145—60.
19. *Zhang D, Liu L, Wang J, et al., and Liu M.* Drug-loaded PEG-PLGA nanoparticles for cancer treatment. *Front Pharmacol.* 2022; **13**:990505.
20. *Wang M, Yu F, Zhang Y.* Present and future of cancer nano-immunotherapy: opportunities, obstacles and challenges. *Mol Cancer.* 2025; **24**(1):26.
21. *Choi Y, Yoon HY, Kim J, et al., and Kim K.* Doxorubicin-Loaded PLGA Nanoparticles for Cancer Therapy: Molecular Weight Effect of PLGA in Doxorubicin Release for Controlling Immunogenic Cell Death. *Pharmaceutics.* 2020; **12**(12):1165.
22. *Gao J, Wang WQ, Pei Q, et al., and Yu HJ.* Engineering nanomedicines through boosting immunogenic cell death for improved cancer immunotherapy. *Acta Pharmacol Sin.* 2020; **41**(7):986—94.
23. *Shi J, Kantoff PW, Wooster R, Farokhzad OC.* Cancer nanomedicine: progress, challenges and opportunities. *Nat Rev Cancer.* 2017; **17**(1):20—37.
24. *Fang RH, Kroll AV, Gao W, Zhang L.* Cell membrane coating nanotechnology. *Adv Mater.* 2018; **30**(23):1706759.
25. *Li J, Wang Y, Liang R, et al., and Zhou J.* Recent advances in targeted nanoparticles drug delivery to melanoma. *Front Oncol.* 2022; **12**:841308.
26. *Wang H, Agarwal P, Zhao S, Xu RX.* Multifunctional nanoparticles in combination immunotherapy. *Nanomedicine (Lond).* 2020; **15**(3):293—308.
27. *Huang X, Zhang F, Lee S, et al., and Chen X.* Long-term multimodal imaging of tumor draining sentinel lymph nodes using mesoporous silica-based nanoprobes. *Biomaterials.* 2012; **33**(17):4370—8.

Received: 22.09.2025
Accepted: 24.03.2026
Published: 14.04.2026

М.Д. Джаффер, А.М. Чалуп
Коледж енергетики та екологічних наук, Науковий університет Аль-Карх
Багдад, Ірак
marwa.dawood@kus.edu.iq

НАНОЧАСТИНКИ «ДОКСОРУБІЦИН-PLGA» — ІМУНОМОДУЛЮЮЧІ ПРОТИПУХЛИННІ ТЕРАПЕВТИЧНІ ЗАСОБИ З ПОДВІЙНОЮ ЦИТОТОКСИЧНОЮ ТА ІМУНОСТИМУЛЮЮЧОЮ ДІЄЮ

Мета. Це дослідження мало на меті дослідити імуномодулюючу та протипухлинну дію наночастинок полі(лактид-ко-гліколевої кислоти), завантажених доксорубіцином (DOX-PLGA NPs), розроблених як наноімунотерапевтична система з подвійною функцією. ***Методи.*** Наночастинки DOX-PLGA були синтезовані методом випаровування емульсії-розчинника та охарактеризовані за розміром частинок, дзета-потенціалом, морфологією (ТЕМ), завантаженням лікарського засобу та поведінкою вивільнення. Цитотоксичність вільних наночастинок DOX та наночастинок DOX-PLGA була оцінена в лініях ракових клітин MCF-7 та HCT116 за допомогою МТТ-аналізу. Ко-культури «мононуклеарні клітини периферичної крові (PBMC) — пухлина» були проаналізовані на секрецію цитокінів (IFN-γ, IL-2, TNF-α та IL-10) та субпопуляції імунних клітин (CD8+ Т-клітини, NK-клітини та поляризація макрофагів). Терапевтичну ефективність було додатково досліджено на мишах з пухлинами CT26. ***Результати.*** Наночастинки DOX-PLGA мали середній розмір приблизно 145 нм (PDI 0,18, ζ −22 мВ), з ефективністю завантаження препарату 12,5% та ефективністю інкапсуляції 78%. Порівняно з вільним DOX, наноформула знижувала життєздатність клітин у більшій мірі ($p < 0,01$) та стимулювала більше вивільнення IFN-γ, IL-2 та TNF-α, тоді як рівень IL-10 знижувався. Проточний цитометричний аналіз показав збільшення популяцій CD8+ Т- та NK-клітин та конгруентне перетворення макрофагів на фенотип M1. Ріст пухлини був значно пригнічений, виживання було подовжено, а наночастинки DOX-PLGA викликали незначну системну токсичність в умовах *in vivo*. ***Висновки.*** Імунонаночастинки демонструють контрольоване вивільнення наночастинок DOX-PLGA, зберігаючи при цьому потужну імуностимуляцію завдяки подвійній цитотоксичній та імуностимулюючій дії. Їхнє застосування як нової платформи для наноімунотерапії в лікуванні раку є виправданим.

***Ключові слова*:** наночастинки PLGA, завантажені DOX; PLGA; наноімунотерапія; цитокіни; імунна активація; терапія раку.